Raman study of rusty oil spotted glaze produced in Linfen kilns (Shanxi province, AD 1115–1368)

Minli Wang, Tian Wang, Fen Wang, Clement Hole, Jun Cao, Jianfeng Zhu, Pei Zhang, Pei Shi, Philippe Sciau

Raman study of rusty oil spotted glaze produced in Linfen kilns (Shanxi province, AD 1115-1368)

Minli Wang[a], Tian Wang[a*], Fen Wang[a], Clement Hole[b], Jun Cao[c], Jianfeng Zhu[a], Pei Zhang[a], Pei Shi[a], Philippe Sciau[b,a,*]

[a] Institute of Silicate Cultural Heritage, School of Material Science and Engineering, Shaanxi Key Laboratory of Green Preparation and Functionalization for Inorganic Materials, Shaanxi University of Science and Technology, 710021 Xi'an, China.
[b] CNRS, CEMES, Toulouse University, 31055 Toulouse, France.
[c] Linfen Museum, 041000 Linfen, China.

E-mail: wangtian@sust.edu.cn; philippe.sciau@cemes.fr

Abstract: The Linfen kiln complex, one of the most representative of Shanxi kilns, is famous for its oil spotted glazed ware production. In this work, micro-Raman spectroscopy was applied to analyze the nature of the rusty oil spot pattern of a bowl fragment from Linfen kilns. Crystals of polygonal shape found in the spots at the glaze surface and around bubbles in the cross-section of the glaze were identified as hematite. Their distribution in the glaze suggests that nucleation seeds and small crystals are carried toward the surface by the rise of bubbles during the heating step of the firing. Raman spectra combined with EDS measurements also suggest that Fe ions in hematite crystals are partially substituted, causing the variation of band position and FWHM of the spectra. Dendritic ε-Fe_2O_3 was identified in brown areas of the black glaze, as well as pseudobrookite crystals of tens of microns in the cross-section of the glaze. The degree of the glaze polymerization (A_{500}/A_{1000}) was calculated at 1.85, indicating a firing temperature lower than 1300°C, consistent with the archaeological data.

Keywords: Linfen kilns, microstructure, hematite, ε-Fe_2O_3, pseudobrookite

1 | INTRODUCTION

Oil spotted glaze is an iron-rich lustrous black glaze decorated with spots resembling drops of oil in water, hence the name oil spotted ware. The spots can vary in color from silvery white to red or rust (the latter cases often referred to as rusty oil spots).[1] Oil spotted glazes play a significant role in the history of ancient Chinese black ceramics. They first appeared during the Song Dynasty (AD 960-1279) in the Jian kilns (Fujian province), which manufactured several types of precious tea bowls including oil spotted glazed bowls, and quickly reached their maturity. The popularity of these bowls also reached Japan, where they were exported by Buddhist monks.[2]

DOI: 10.1002/jrs.6229

Their popularity and preciousness led many northern kiln complexes, such as the Ding kilns (Hebei province), Hebi kilns (Henan province), Linfen kilns, Jiexiu kilns or Hunyuan kilns (Shanxi province), to compete to imitate Jian oil spotted wares.[3] Among these northern complexes, the Linfen kilns were one of the most famous kilns due to their large production and high demand during the Jin and Yuan periods (AD 1115-1368).[3]

Many studies were carried out to understand the formation process and color variation of the oil spot pattern.[4–11] It is believed that this pattern comes from local iron enrichment during the firing, which results in locally iron-supersaturated glaze leading to local crystallization of iron oxides, such as hematite (α-Fe_2O_3), magnetite (Fe_3O_4)[5,9] or ε-Fe_2O_3[4,6] during cooling stage. The silvery shine of Jian oil spotted wares is hypothesized to come from ε-Fe_2O_3 crystals of several micrometers in size organized in a periodic two dimensional fashion.[6] Studies about oil spotted glazes were mainly devoted to the more famous Jian wares [6,9] or replicated production [7,8,10,11] but few focused on Linfen wares and the rusty oil spot pattern.

Micro-Raman spectroscopy is a suited technique to investigate micro-crystalline phases in the glazes of ancient ceramics thanks to the micro-scale of the probe and its high sensitivity. This technique enable a precise discrimination of the different iron oxides, such as hematite,[12] maghemite (γ-Fe_2O_3),[13] ε-Fe_2O_3[14] and magnetite[15] at very low laser power (less than 1 mW) and without any strong influence from glassy matrix. The non-destructiveness of this technique is also perfectly suited for analyzing precious and ancient artifacts.

In this work, a representative fragment of Linfen rusty oil spotted glazed ware was selected and analyzed to determine the chemical nature of the pattern and its surrounding black glaze using micro-Raman spectroscopy combined with XRF, optical microscopy and SEM-EDS. Based on the results, the formation process and chemical influence on the color of the oil spotted glaze are discussed.

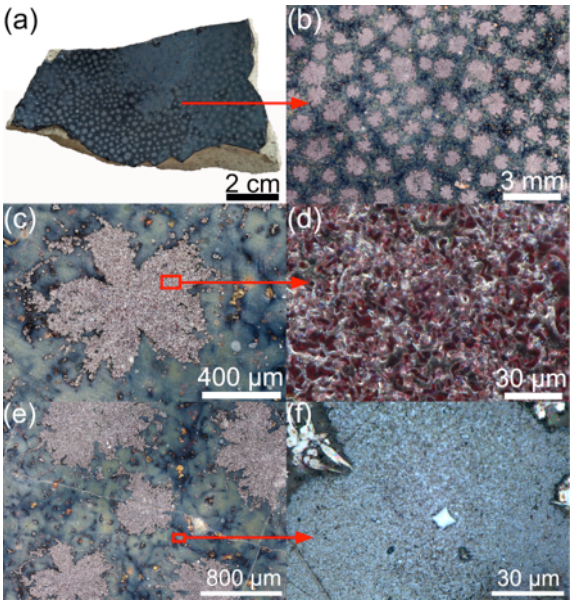

Figure 1 *Oil spotted fragment excavated in Linfen kilns (a), with the corresponding optical observation of the oil spot pattern under X20 (b), X200 (c) and X2500 (d) magnification (ring light source) and the light brown zone of the glaze under X100 (e, ring light source) and X2500 (f, coaxial light source) magnification*

2 | MATERIALS AND METHODS

2.1 | Sample description

The rusty oil spotted glazed fragment studied is presented in Figure 1a. It was excavated from Linfen kilns in Shanxi Province and can be dated from the Jin or Yuan Dynasty (AD 1115-1368) according to its archaeological context. It is characterized by a highly glossy black glaze decorated with rusty oil spots, which is

DOI: 10.1002/jrs.6229

consistent with features of a typical oil spotted bowls from the Linfen kilns.[1]

2.2 | Analytical techniques and conditions

Optical microscopy equipped with an ultra-depth-of-field system was implemented to observe the oil spotted glaze surface. X-ray fluorescence spectroscopy was performed on the glaze surface and body. Scanning electron microscopy coupled with energy dispersive spectrometry and micro-Raman spectroscopy were implemented on the surface and a cross-section of the glaze. The preparation process of the cross-section is described elsewhere.[16]

2.2.1 | Optical microscopy equipped with an ultra-depth-of-field system

Optical imaging of the glaze surface was performed using a KEYENCE optical microscope equipped with a surface depth observation system (VHX-7000). Images were taken with a magnification ranging from x20 to x2500. Ring and coaxial light sources were used to observe the surface coloration and particle distribution in the glaze of the sample.

2.2.2 | X-ray fluorescence spectroscopy (XRF)

Elemental composition of the oil spotted ware was determined by energy dispersive X-ray fluorescence (EDXRF, XGT-7200, Horiba) equipped with an optical microscope to select the zones of interest. Measurements were carried out under vacuum and the X-ray tube voltage was 50 kV. Acquisition time was set to 120s for each point and the incident X-ray beam diameter was 1.2 mm. A minimum of three spectra was recorded on the glaze surface and the body to estimate their homogeneity.

2.2.3 | Scanning electron microscopy and energy dispersive spectrometry (SEM-EDS)

Prior to SEM-EDS analyses, the surface and cross-section of the sample were coated with a thin layer of gold to enhance their conductivity. The morphology and elemental composition of crystals in the glaze were investigated using a scanning electron microscope (FEI Apreo LoVac) equipped with an energy dispersive X-ray spectrometer analysis system (EDAX Octane Elect Super). EDS spatial resolution was around 0.2 μm. The Origin software was utilized to analyze the corresponding EDS spectra.

2.4 | Micro-Raman spectroscopy

Micro-Raman spectroscopy was performed on the surface and the cross-section of the glaze at room temperature using the Renishaw inVia spectrometer with a Peltier cooled CCD detector. 532 nm excitation was provided by a solid-state laser with a spot size of about 2-3 μm in diameter and a power inferior to 1 mW to optimize the signal/background ratio and avoid any thermal effect. Collection time of 100 s for each spectrum was chosen to obtain a refined resolution inferior to 1 cm^{-1}. Igor software was used for data treatment. The intelligent polynomial baseline was selected to subtract the photoluminescence background and the polynomial order

DOI: 10.1002/jrs.6229

was defaulted to be 11. Minimum smoothing was performed to obtain the optimal spectral curves.

3 | RESULTS

3.1 | Elemental composition

Table S1 shows the elemental compositions recorded on the oil spots, surrounding black glaze and body of the sample. The main constituents of the glaze are SiO_2 (~69.1%), Al_2O_3 (~14.6%), CaO (~4.9%) and Fe_2O_3 (~5.1%). The MgO content is around 2.90% and K_2O amount is about 1.85%. Small amounts of Na_2O (~0.6%), TiO_2 (~0.8%) and MnO_2 (~0.1%) were also detected. The elemental composition recorded on the spots is relatively similar to the one of the black glaze, the only difference being the slightly higher iron concentration in the spots. The similarity can be explained by the fact that the analyzed area of XRF is around 1.2 mm, thus could not be precisely positioned on the oil spots, whose sizes vary from 0.4 to 1.4 mm (Fig. 1). The body contains more Al_2O_3 and less SiO_2, CaO and Fe_2O_3 than the glaze.

Oil spotted glaze	SiO_2	Al_2O_3	Fe_2O_3	CaO	K_2O	MgO	TiO_2	MnO	Na_2O	P_2O_5	∑[M]/∑[Al]+[Si]
This work (15 pts)	68.68 (0.80)	14.29 (0.27)	5.85 (0.59)	4.71 (0.12)	1.86 (0.07)	2.98 (0.18)	0.88 (0.06)	0.09 (0.01)	0.66 (0.50)	0.00 (0.00)	0.14
Linfen kilns	68.82	13.42	5.23	4.29	4.33	1.89	0.87	0.09	1.05	0.00	0.14
Jian kilns	69.85	15.68	3.42	4.92	3.22	0.70	0.50	0.40	0.40	0.90	0.11
Jiexiu kilns	65.21	15.13	5.82	6.25	2.59	2.67	0.89	0.09	1.20	0.15	0.17
Xiao kilns	68.34	12.17	5.28	7.45	3.13	1.73	0.76	0.25	0.25	0.65	0.17

Table 1 Analytical results (wt%) obtained by X-ray fluorescence on the glaze surface (standard variations in brackets) compared with ones of oil spotted glaze wares of Linfen kilns (Shanxi province), Jian kilns (Fujian province), Jiexiu kilns (Shanxi province) and Xiao kilns (Anhui province) [4]. The mole ratios of the glaze modifiers (∑[1/2Na_2O+MgO+1/2K_2O+CaO+1/2Fe_2O_3]) to network form (∑[1/2Al_2O_3+SiO_2]) of OS glazes were calculated, abbreviated as ∑M/∑[Al]+[Si].

The main analytical results (wt%) reported in the literature[4] on oil spotted glazes from different kilns are given in Table 1. The major elements found in the present sample are consistent with the recordings of wares from Linfen kilns. SiO_2 and Al_2O_3 concentrations are around 68.7-68.8% and between 13.4-14.3%, respectively. The glaze presents a relatively high CaO concentration (4.3-4.7%). Only differences in K_2O (relatively lower than the concentrations reported in the literature[4]) and MgO (slightly higher than the concentrations reported[4]) were observed. Compared with fragments from different kilns, fragments from Linfen, Jian and Xiao kilns present slightly higher SiO_2 (68.3-69.9%) than the ones from Jiexiu kilns (65.2%). Fragments from Linfen and Xiao kilns present slightly lower Al_2O_3 amount (12.2-14.3%) than ones of Jian and Jiexiu kilns (15.1-15.7%). The glaze modifiers (Na_2O, MgO, K_2O, CaO ...) concentrations in wares from different kilns are more various from one to another. In order to precisely discuss their variations, the molar ratios of the glaze modifiers (∑[1/2Na_2O+MgO+1/2K_2O+CaO+1/2Fe_2O_3]) to the network formers (∑[1/2Al_2O_3+SiO_2]) of oil spotted glazes were calculated. The ratio of the glaze from Linfen kilns calculated around 0.14 is consistent with previous reports averaging around 0.15. It can be noted that oil spotted glazes from Jiexiu and Xiao kilns (Anhui province) present a slightly higher ∑[M]/∑[Al]+[Si] ratio (~0.17) than the Jian wares,

DOI: 10.1002/jrs.6229

which is the lowest at ~0.11, indicating than the firing temperature needed to manufacture Jian wares might be slightly higher than the one needed for the wares from other kilns, according to the theory of silica-rich and modifier (Na, K, Ca,…)-poor compositions corresponding to high firing temperature.[17,18] However, since the different ratios between the kilns are relatively similar and the analytical accuracy was not fully taken in account, one should be particularly cautious with these ratios.

3.2 | Morphological analyses

Low magnification optical microscopic imaging of the glaze surface (Fig.1a and b) reveals the relatively homogeneous distribution of the spots on the glaze. It also highlights that the black glaze contains many light brown areas. The spots are crimson in color and their size varies from 0.4 to 1.4 mm (Fig. 1b and c). Imaging at greater magnification (x2500) under a ring light source reveals that they are composed of many crimson polygonal-shaped crystals of several microns in size (Fig. 1d). Conversely, the light brown areas contain many small shiny crystals according to x2500 magnification imaging under a coaxial light source (Fig. 1e and f).

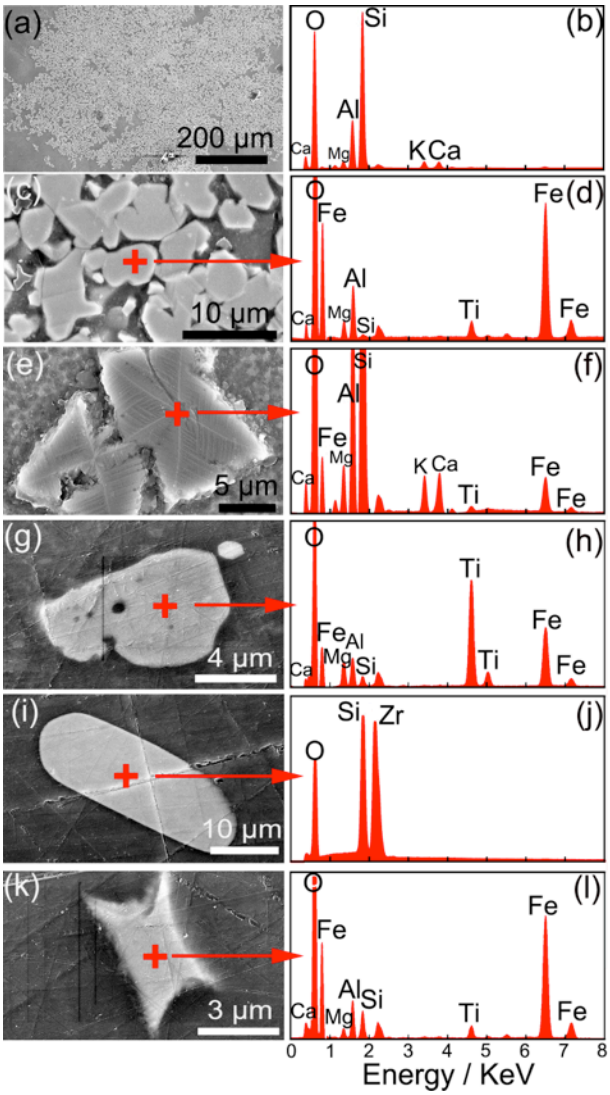

Figure 2 *SEM-BSE images of one oil spot under low magnification (a), particles on the glaze surface (c and e) and in the cross-section (g, i and k) at higher magnification. EDS spectra recorded on the glassy matrix in a black area (b) and on the different crystalline structures observed by SEM-BSE (d, f, h, j and l).*

SEM-BSE imaging and EDS analyses were performed on the glassy matrix, polygonal crystals in the oil spots and the shining crystals in the light brown areas (Fig. 2). Fig. 2a shows one oil spot in the glaze at low magnification. Higher magnification imaging of the crystals from this spot confirms that the small polygonal crystals constitute of the oil spot pattern (Fig. 2c). The shiny crystals found in the light brown zones of the glaze (Fig. 1f) are dendrites of several microns (Fig. 2e). EDS analyses were performed on the glassy matrix (Fig. 2b), the polygonal crystals in the oil spots (Fig. 2d) and the dendritic crystals in the brown areas (Fig. 2f). Analytical results shown in Table 2 highlight that the polygonal crystals contain mainly Fe, O and a little Ti, with a Ti/Fe ratio of about 0.07 (Fig. 2d and

DOI: 10.1002/jrs.6229

Table 2). The Ti concentration found in the crystals, albeit relatively low, is higher than in the glassy matrix, confirming that the crystals indeed contain Ti (Table 2). The dendritic crystals are composed of Fe and O (Fig. 2f and Table 2). As the glassy matrix is relatively rich in Si, Al, Ca, K and Mg (Fig. 2b and Table 2), the signals of other elements detected in the spectra of these crystals (Fig.2d and Fig. 2f) probably come from the glassy matrix.

Glaze	Crystal	Mg	Al	Si	K	Ca	Ti	Mn	Fe	Zr	Ti/Fe
Surface	Polygon	4.45	9.87	1.71	0.43	0.46	5.48	0.50	77.1	-	0.07
	Dendritic	4.47	16.4	48.4	5.15	7.04	1.35	0.52	16.7		-
	Glassy Matrix	4.56	18.9	58.7	6.59	5.59	2.39	0.49	2.76	-	0.87
Cross section	Ellipse	4.90	4.13	49.7	0.98	0.65	0.51	1.40	1.89	35.9	-
	Psb_1	6.40	19.5	1.44	0.26	0.25	45.1	0.30	26.7	-	1.69
	Psb_2	7.02	7.17	2.23	0.37	0.35	43.0	0.34	39.5	-	1.09
	Psb_3	4.93	16.4	2.66	0.36	0.28	42.1	0.27	32.9	-	1.28
	$Star_1$	2.99	7.93	4.83	0.48	0.56	4.80	0.61	77.8	-	0.06
	$Star_2$	3.04	8.86	7.64	0.59	0.86	4.52	0.51	73.9	-	0.06

Table 2 *Analytical results (atom%) obtained by EDS spectrometry on crystals observed on the glaze surface and the cross-section by SEM. Chemical compositions of polygonal and dendritic crystals as well as the glassy matrix at the surface were obtained from the EDS spectra shown in Fig. 2d, 2f and 2b respectively. Chemical composition of ellipse, Psb_1 and $Star_1$ crystals in the glaze cross-section were obtained from the EDS spectra of Fig. 2h, 2j and 2l respectively.*

SEM-EDS analyses were also implemented on the cross-section of the glaze of the sample. Fig. S1a shows that the thickness of glaze is around 740 μm and that it contains many bubbles with size varying from 14 to 150 μm (Fig. S1b). Polygonal crystals of several microns, similar to the ones observed at the surface of the glaze, were also observed around the bubbles (Fig. S1c). Several different crystals of tens of microns were also discovered around some bubbles (Fig. 2g and Fig. S1d). The corresponding EDS results (Fig. 2h) show that these crystals contain mainly Fe and Ti with an atomic Ti/Fe ratio varying from 1.1 to 1.7 (labeled as Psb_1, Psb_2 and Psb_3 in Table 2 for pseudobrookite). One large elliptical crystal was found in the cross-section of the glaze (Fig. 2i). According to the EDS analysis (Fig. 2j), it is rich in Si, Zr and O, with a Si/Zr ratio close to 1 (Table 2) a. Several star-shaped crystals (labeled as $Star_1$ and $Star_2$, Table 2) were also observed in the cross-section of the glaze (Fig. 2k). They contain mainly Fe and a small quantity of Ti, with Ti/Fe ratios around 0.06 according to EDS analyses (Fig. 2l).

3.3 | Structural analyses

Micro-Raman spectroscopy was implemented to identify the different crystals observed both at the surface of the glaze and in its cross-section. Spectra recorded on the crimson polygonal crystals found in the rusty oil spots (Fig. 1d and Fig. 2c) and around the bubbles in the cross-section of the glaze (red cross in Fig. S1c) are characteristic of hematite, with typical peaks around 231 cm^{-1}, 297 cm^{-1}, 413 cm^{-1} and 1337 cm^{-1} (Fig. 3a).[12] An additional peak around 674 cm^{-1}, not typical of hematite, was also observed. This peak has been previously observed in Ti- and Al-substituted hematite.[19] Such attribution may be relevant to consider in this case as EDS measurements revealed the presence of Ti in these crystals. As for Al, its presence

DOI: 10.1002/jrs.6229

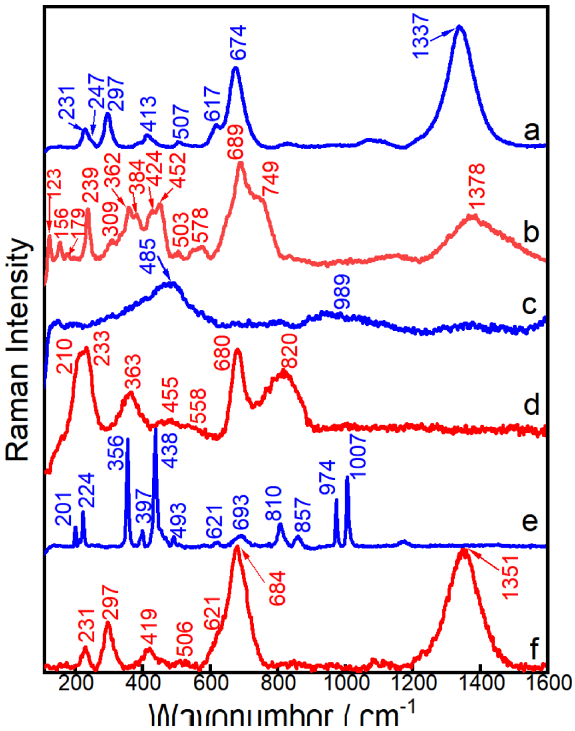

Figure 3 *Raman spectra recorded on hematite (a) and ε-Fe_2O_3 (b) crystals (corresponding to the crystals shown in Fig. 2c and e, respectively) and black area of the glaze surface (c). Raman spectra recorded on pseudobrookite (d), zircon (e) and hematite (f) crystals found in the cross-section of the glaze (corresponding to the crystals shown in Fig. 2g, i and k, respectively).*

as a substituting element in the crystals cannot be confirmed by SEM-EDS analysis because the glassy matrix contains a significant level of Al and the analyzed volume cannot be limited to the crystals (Fig. 2d). The dendritic crystals found in the light brown zone of the glaze surface (Fig. 1f and Fig. 2e) have spectral characteristics of ε-Fe_2O_3 phase (Fig. 3b), i.e., 123, 156, 179, 239, 309, 362, 384, 424, 452, 503, 578, 689, 749 and 1378 cm^{-1}, similar to spectra recorded on oil spotted wares from the Jian kilns.[6] Spectra recorded on an area without crystals at the glaze surface have two broadened bands at ~500 cm^{-1} and ~1000 cm^{-1} (Fig. 3c) which could be attributed to the bending and stretching modes of [SiO_4] tetrahedron, respectively.[18] The calculated area ratio of these two bands is 1.85, suggesting that the firing temperature was lower than 1300°C.[16–18] The large crystals mainly located around the bubbles in the cross-section of the glaze (Fig. S1d and Fig. 2g) were identified as pseudobrookite (Fe_2TiO_5) (Fig. 3d) by comparison with a spectrum (No. R050563) from the RRuFF database (Fig. 4), consistently with EDS analyses (Fig. 2h). The large elliptical crystal found in the cross-section of the glaze (Fig. 2i) presents typical Raman features of zircon ($ZrSiO_4$) (Fig. 3e),[20] which is consistent with the EDS-analyses (Fig. 2j). The star-shaped crystals found in the cross-section of the glaze (Fig. 2k) present similar Raman features (Fig. 3f) to the ones of polygonal crystals (Fig. 3a), including an additional peak around 684 cm^{-1} which were identified as hematite with probable substitutions.[19]

In addition some crystalline clusters were observed in the cross-section of the glaze (Fig. S2) and were identified as a mixture of hematite (Fig. S2, pt01)[12] and pseudobrookite (Fig. S2, pt02).[19] A summary of the observed crystals at the surface and in the cross-section of the glaze are listed in the Table 3.

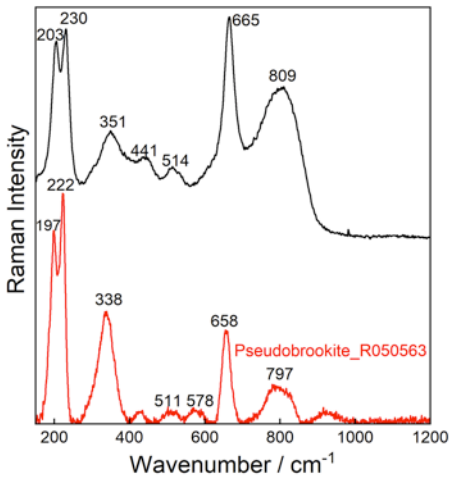

Figure 4 *Comparison of the Raman spectrum recorded on one pseudobrookite crystal in the cross-section of the glaze with the spectrum of pseudobrookite (Fe_2TiO_5, No. R050563) from the RRuFF database.*

DOI: 10.1002/jrs.6229

To further study the influence of the Ti/Fe ratio on the Raman spectra of pseudobrookite crystals, analyses of the variation of the position and FWHM (Full Width at Half Maximum) of the bands at ca. 660-690 cm^{-1} were performed. A linear relationship between the position and FWHM of the bands could be observed (Fig. 5a). In addition, it was found that both the wavenumber and FWHM were higher the higher the Ti/Fe ratio measured on the crystals was. This suggests that a higher Ti/Fe ratio in the crystals results in a shift toward higher wavenumber and larger peaks. However, as the ratio was measured only for three crystals, the observed tendency has to be considered cautiously.

	Crystalline type	Raman bands / cm^{-1}
Crystals (surface)	Hematite	231 (w), 247 (vw), 297 (s), 413 (w), 507 (vw), 617 (s), 674 (vs), 1337 (vs)
	ε-Fe_2O_3	123 (s), 156 (w), 179 (w), 239(s), 309 (w), 362 (s), 384 (s), 424 (s), 452 (s), 503 (w), 578 (w), 689 (vs), 749 (vs), 1378 (s)
Crystals (cross-section)	Zircon	201 (s), 224 (s), 356 (vs), 397 (s), 438 (vs), 493 (vw), 621 (vw), 693 (w), 810 (s), 857 (w), 974 (vs), 1007 (vs)
	Pseudobrookite	210 (vs), 233 (vs), 363 (s), 455 (w), 558 (w), 680 (vs), 820 (vs)
	Hematite	231 (s), 297 (vs), 419 (s), 506 (vw), 621 (w), 684 (vs), 1351 (vs)

Table 3 *Crystal types detected by Raman spectroscopy in the surface and cross-section of the glaze of the Linfen oil spotted ware. The abbreviation "vw", "w", "s", "vs" in the brackets signifies "very weak", "weak", "strong" and "very strong" respectively, which indicate qualitatively the intensity of each band.*

Similar further study was implemented with the additional peak (ca. 665-690 cm^{-1}) of the Raman spectra of hematite crystals of polygonal and star shape (Fig. 5b). Major discrepancies between the star-shaped and polygonal crystals can be observed, with a peak centered between 673 and 686 cm^{-1} and with an FWHM varying from 47 to 72 cm^{-1} for the polygonal crystals (red triangles in the orange circle, Fig. 5b) and more various features for the star-shaped crystals (blue squares, Fig. 5b). For the latter, the peaks of most of crystals locate at higher wavenumbers

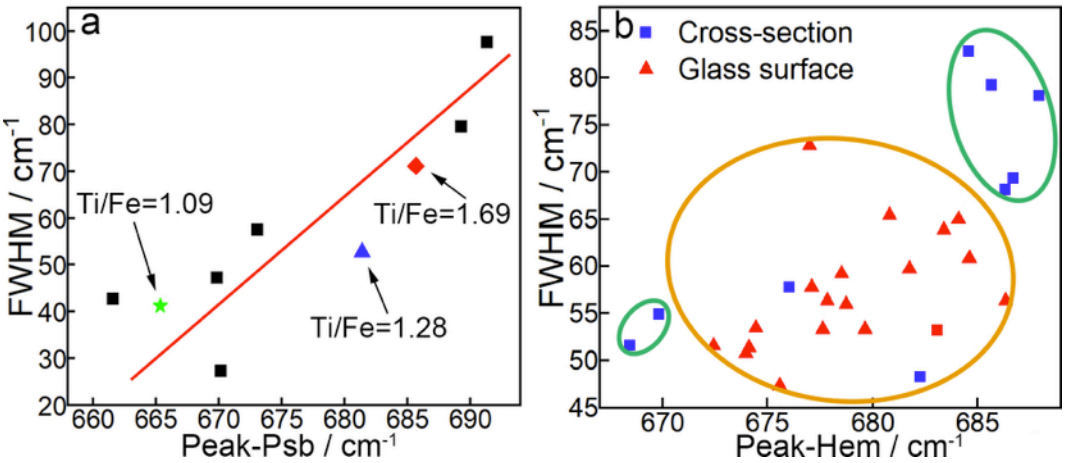

Figure 5 *(a) Graphical representation of the position versus the full width at half maximum (FWHM) of the pseudobrookite peak around 680 cm^{-1} observed in the cross-section of the glaze. Ti/Fe ratios of three pseudobrookite crystals were calculated from the corresponding EDS results. (b) Graphical representation of the position versus FWHM of the hematite peak around 680 cm^{-1}. Peaks from spectra recorded on crystals from the surface of the glaze are indicated asred triangles and on crystals from the cross-section as blue squares.*

DOI: 10.1002/jrs.6229

(centered at 684-689 cm^{-1}) and have larger FWHM values (69-84 cm^{-1}) (blue squares in the green circle, Fig. 5b). Four star-shaped crystals also observed present relatively low FWHM value (48-57 cm^{-1}) and Raman shifts than the other. Two of them are in the same region than the polygonal crystals (blue squares in the orange circle, Fig. 5b) and the peaks of the other two at even lower wavenumbers (668 and 670 cm^{-1}) (green circle, Fig. 5b). Unfortunately, no clear relation among those features and the Ti/Fe ratio can be highlighted. The small size of these crystals and the presence of Ti in the glassy matrix surrounding them prevent accurate measurement of their low Ti concentration allowing the linkage of their Ti/Fe ratio to their FWHM or wavenumber shifts. However, the shifts in wavenumber and the FWHM variation of the main hematite peaks (the broadening of the doublet at 231-297 cm^{-1} and the shits of the bands at ~413 cm^{-1} and ~1300-1400 cm^{-1}) caused by the level of substitution of Fe ions was significant and consistent with previous works.[21,22]

4 | Discussion

According to the morphology and structure of the hematite crystals found in the oil spots and around the bubbles, a possible formation mechanism of the oil spot pattern is proposed in Fig. 6. Hematite nucleation seeds are first formed at the gas-liquid interface of the bubbles inside the glaze during the firing at high temperature (<1300 °C) (Fig. 6a). They progressively accumulate around the growing bubbles, which move within the glassy matrix toward the surface carrying with them the small hematite crystals. During this step, some iron oxides might react with titanium oxides present within the glaze to form pseudobrookite crystals observed around the bubbles (Fig. 6b). The rest that reach the surface grows to give the spots of different sizes that characterize the rusty oil spot pattern (Fig. 6c). Contrary to the oil spotted ware from the Jian kilns,[6] which display dendritic structure hypothesized to come from a dissolution of the iron oxides during firing followed by a re-crystallization during cooling, the polygonal shape of the crystals of this sample suggest that their growth began during the heating step. In addition, the spots of this Linfen ware fragment are flower-shaped with well-defined boundary (Fig. 1b and c) instead of being round, such as those found on Jian wares.[6]

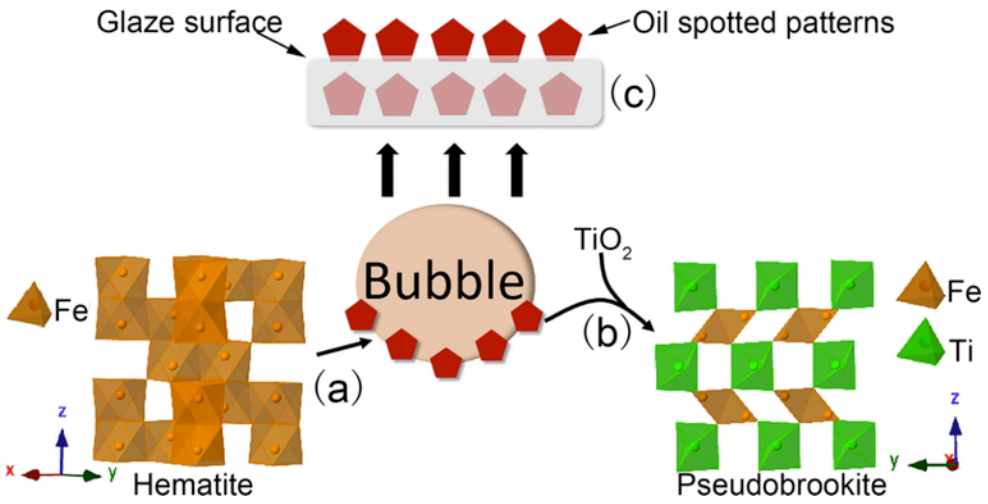

Figure 6 *Schematic diagram of growth process of oil spot pattern on the black glaze.*

DOI: 10.1002/jrs.6229

The crimson color of the rusty oil spotted pattern is probably the result of the concentration of polygonal hematite crystals of several microns in the spots. The dark shade of the crystals is typical of the diffuse color of hematite crystals of this size.[23] The substitution of some Fe ions by Ti ions and other elements might also influence the color of the hematite crystals: Ti[19] has been reported to usually darken the color of hematite, however probable Al substitution which could not be verified due to the high Al concentration in the glassy matrix could counterbalance this darkening. The global crimson aspect of the spots can be explained by the diversity of crystalline orientation of the crystals, which prevents highly reflective effects and favors the crimson diffused color of the crystals.

The brown areas found in the black glaze may be explained by the presence of the rare ε-Fe_2O_3 polymorph. It has been already documented in several black-to-brown Chinese glazes, such as oil spotted and hare's fur wares from the Jian kilns (southern Song dynasty),[6,25] sauce wares from the Yaozhou kilns (Shaanxi province, northern Song dynasty),[26] purple-gold wares from the Jingdezhen kilns (Jiangxi province, Qing dynasty)[27] and sauce glaze from the Qilizhen kilns (Jiangxi province, southern Song dynasty).[28]

Zircon was also found in the glaze and was also observed in other glazes from Yaozhou hare's fur wares[29] and celadons.[16] This very stable mineral with a high melting point (>2430 °C) is common in sediments such as those used to produce the wares, so it probably comes from the raw materials used. The EDS spectrum (Fig. 2h) recorded on the crystals shows that it is pure, similarly to the ones found in Yaozhou hare's fur wares[27] and celadons.[16]

5 | Conclusions

The surface and cross-section of a Linfen rusty oil spotted bowl sherd were analyzed by micro-Raman spectroscopy, XRF and SEM-EDS. The glaze surface is composed of the oil spot pattern on brown and black areas, which present all three similar elemental composition, except for a slightly higher Fe concentration in the spots. The spots are composed of polygonal-shaped hematite crystals. Ti-substitution has been detected in the hematite crystals (according to EDS results). Al-substitution is also probable, however its high concentration in the glassy matrix does not allow certainty. The accumulation and diversity of orientation of the substituted hematite crystals may explain the crimson color of the oil spots. Similar crystals were also observed in the cross-section of the glaze, at the interface between bubbles and glaze, suggesting that hematite seeds are first formed in the glaze during the heating step and are transported toward the surface by the bubbles rather than directly formed on the glaze surface. Mixtures of hematite and pseudobrookite crystals, as well as isolated pseudobrookite crystals were observed in the cross-section of the glaze, suggesting that pseudobrookite crystals might come from a reaction between hematite and titanium oxides. Besides, the brown areas of the glaze has been associated with the presence of small dendritic ε-Fe_2O_3 crystals.

DOI: 10.1002/jrs.6229

Acknowledgement

This work has been financially supported by China National Key R&D Program (No. 2019YFC1520202 and No. 2019YFC1520103), China National Natural Science Foundations (No. 51972201 and No. 51902192), Shaanxi Natural Science Basic Research Projects (No. 2021JZY-014 and No. 2020JQ-721) and Silicate Cultural Heritage Protection and Utilization Innovation Team of Shaanxi Province (No. 2020TD-008). It was also supported by the PHC CAI YUANPEI project (No° 46284PB). It was performed in the framework of the research collaboration agreement (CNRS No. 186116) between the French National Centre for Scientific Research and the Shaanxi University of Science and Technology.

References

[1] J. Z. Li, *History of Science and Technology in China, Ceramics Volume*, Science Press, Beijing, **1998**.

[2] J. Sun, *Research on the restoration of of Jian bowl of Jian kiln complex,* China Literary Federation Press, Beijing, **2016.**

[3] F. Zhang, *The Science of Ancient Chinese Ceramics*, Shanghai People's Fine Arts Press, Shanghai People's Fine Arts Publishing House, Shanghai, **2000**.

[4] Y. Xu, Y. Qin, F. Ding, *Ceram. Int.* **2017**, *43*, 8636.

[5] X. Li, J. Lu, X. Yu, J. Zhou, L. Li, *Ceram. Int.* **2016**, *42*, 15269.

[6] C. Dejoie, P. Sciau, W. Li, L. Noé, A. Mehta, K. Chen, H. Luo, M. Kunz, N. Tamura, Z. Liu, *Sci. Rep.* **2014**, *4*, 4941/1.

[7] X. Wang, *Shandong Taoci (Shandong Ceramics).* **2018**, *42*, 32.

[8] Y. Wu, J. Du, J. Zhu, D. Huang, *Bull. Chin. Ceram. Soc.* **2017**, *36*, 374.

[9] Z. Lin, *J. Chin. Ceram. Soc.* **1979**, *7*, 190.

[10] J. Wang, W. Liu, B. Liu, Z. Li, *Ceramics Engineering*. **2001**, 13.

[11] X. He, X. Lu, C. Cao, H. Shen, Y. Chen, B. He, Y. Bao, *J. Ceram*. **2017**, *38*, 173.

[12] C. P. Marshall, W. J. B. Dufresne, C. J. Rufledt, *J. Raman Spectrosc.* **2020**, *51*, 1522.

[13] P. P. C. Sartoratto, K. L. Caiado, R. C. Pedroza, S. W. da Silva, P. C. Morais, *J. Alloys Compd.* **2007**, *434–435*, 650.

[14] J. Lopez Sanchez, A. Serrano, A. Del Campo, M. Abuín, O. Rodríguez de la Fuente, N. Carmona, *Chem. Mater.* **2015**, *18*, 511.

[15] L. Y. Novoselova, *Appl. Surf. Sci.* **2021**, *539*, 148275.

[16] T. Wang, P. Chen, M. Wang, Z. Sang, P. Zhang, F. Wang, P. Sciau, *J. Eur. Ceram. Soc.* **2020**, *40*, 4676.

[17] P. Colomban, *J. Non-Cryst. Solids* **2003**, *323*, 180.

[18] P. Colomban, O. Paulsen, *J. Am. Ceram. Soc.* **2005**, *88*, 390.

[19] T. Wang, C. Sanchez, J. Groenen, P. Sciau, *J. Raman Spectrosc.* **2016**, *47*, 1522.

[20] L. D. Kock, M. D. S. Lekgoathi, E. Snyders, J. B. Wagener, J. T. Nel, J. L. Havenga, *J. Raman Spectrosc.* **2012**, *43*, 769.

[21] F. Froment, A. Tournié, P. Colomban, *J. Raman Spectrosc.* **2008**, *39*, 560.

[22] G. Simsek, P. Colomban, F. Casadio, L. Bellot-Gurlet, G. Zelleke, K. T. Faber, V.

DOI: 10.1002/jrs.6229

Milande, L. Tilliard, *J. Am. Ceram. Soc.* **2015**, *98*, 3006.
[23] J. Wang, W. B. White, J. H. Adair, *J. Am. Ceram. Soc.* **2005**, *88*, 3449.
[24] H. Inada, T. Hosoya, Y. Okazaki, Y. Arakawa, T. Takaishi, H. Hasimoto, *J. Eur. Ceram. Soc.* **2020**, *40*, 5790.
[25] Q. Hoo, Y. Liang, X. Yan, X. Wang, T. Cao, X. Cao, *J. Eur. Ceram. Soc.* **2020**, *40*, 4340.
[26] R. Wen, D. Wang, L. Wang, Y. Dang, *Ceram. Int.* **2019**, *45*, 10589.
[27] Z. Liu, C. Jia, L. Li, X. Li, L. Ji, L. Wang, Y. Lei, X. Wei, *J. Am. Ceram. Soc.* **2018**, *101*, 5229.
[28] L. Wang, Y. Wang, M. Zhang, Q. Li, J. Wu, Z. Liu, L. Li, X. Wei, *Anal. Chem.* **2019**, *91*, 13054.
[29] W. Li, W. Zhang, X. Lu, N. Zheng, H. Luo, *J. Build. Eng.* **2011**, *14*, 329.

DOI: 10.1002/jrs.6229